

## Catalytic abatement of volatile organic compounds and soot over manganese oxide catalysts

M.J. Marin-Figueroa, C. Cocuzza, S. Bensaid, D. Fino, M. Piumetti\*, N. Russo

Department of Applied Science and Technology, Politecnico di Torino, Corso Duca degli Abruzzi 24, 10129 Torino, Italy.

\*to whom correspondence should be addressed. Tel.: +39-011-0904753; Fax: +39-011-0904699;

Corresponding author e-mail: [marco.piumetti@polito.it](mailto:marco.piumetti@polito.it)

### Abstract

A set of manganese oxide catalysts was synthesized via two preparation techniques, the solution combustion synthesis ( $\text{Mn}_3\text{O}_4/\text{Mn}_2\text{O}_3$ -SCS and  $\text{Mn}_2\text{O}_3$ -SCS) and the sol-gel synthesis ( $\text{Mn}_2\text{O}_3$  – SG550 and  $\text{Mn}_2\text{O}_3$  – SG650). The physico-chemical properties of the prepared catalysts were studied by means of several techniques:  $\text{N}_2$ -physisorption at  $-196$  °C, X-ray powder diffraction,  $\text{H}_2$  temperature-programmed reduction, soot temperature-programmed reduction, X-ray photoelectron spectroscopy (XPS) and field-emission scanning electron microscopy (FESEM). The high catalytic performance of the powder catalysts was verified in the oxidation of VOC probe molecules (ethene and propene) and carbon soot by means of a temperature-programmed oxidation setup. The best catalytic performances in the abatement of soot were observed for the  $\text{Mn}_2\text{O}_3$  – SG550 and the  $\text{Mn}_3\text{O}_4/\text{Mn}_2\text{O}_3$ -SCS catalysts. The catalytic activity in VOC total oxidation was effectively correlated to an enhanced low-temperature reducibility of the catalysts along with the abundant surface  $\text{O}_\alpha$  species. Likewise, the low-temperature oxidation of soot in “tight” contact condition, occurred over the  $\text{Mn}_2\text{O}_3$  – SG550 catalyst and it was attributed to high amount of surface  $\text{O}_\alpha$  species and better surface reducibility. On the other hand, for the soot oxidation in “loose” contact conditions, the improved catalytic performance of the  $\text{Mn}_3\text{O}_4/\text{Mn}_2\text{O}_3$ -SCS catalyst, was attributed to the beneficial effect of both its morphological structure that (resembling a filter) enhances the capture of soot particles, and with a probable high amount of surface acid sites, characteristic of  $\text{Mn}_3\text{O}_4$  catalysts.

**Keywords:** manganese oxide catalysts, soot catalytic oxidation, catalytic oxidation of VOC, sustainable catalysts.

## 1. INTRODUCTION

In the recent years, the elevated concentration of pollutant substances in air increased the occurrence of respiratory diseases and deaths in Europe and worldwide [1-4]. This context encouraged the regulation for the emission of PM and/or VOCs in several countries [5,6]. The volatile organic compounds are a set of substances produced every year by means of either natural processes or as the result of human activities (biogenic and anthropogenic, respectively) [7]. On the other hand, the particulate matter is formed by elemental carbon aggregates with surface adsorbed organic compounds, sulphur and metal oxides. It is formed due to the pyrolysis of hydrocarbons taking place with a defective stoichiometric amount of oxygen that leads to the nucleation of solid particles [8,9].

In order to achieve the emission of acceptable amounts of these pollutants, different abatement technologies have been developed. In order to diminish the VOCs emission techniques like adsorption, thermal oxidation, catalytic oxidation, etc., have been developed [10-17]. Instead, the elimination of carbonaceous particulate matter has been investigated and applied in the automotive sector, e.g. in Diesel particulate filters [18]. Consistently, the catalytic oxidation process has demonstrated its suitability for the elimination of either VOCs or PM by means of active catalysts.

Concerning the elimination of VOCs, many catalytic materials, e.g. noble metals and metal oxides, have been studied. The former materials are usually characterized by a remarkable catalytic performance, but are more expensive and may be subject to poisoning [13,19]. On the other hand, the metal oxides are low-cost materials but have shown to be catalytically active at higher temperatures [10,13]. The enhanced catalytic activity of transition metal oxides, as reported in different research investigations, has been attributed to: high amount of surface chemisorbed oxygen species and enhanced mobility of oxygen (associated with the catalyst reducibility) [20,21], an electron deficient lattice that with enhanced conductivity (i.e. occurrence of positive “holes”), and ability of the metal of assuming variable oxidation states [22]. Manganese is among the most abundant elements in the earth crust [23], therefore it constitutes a potential candidate material for the preparation of sustainable catalytic materials. Previous investigations evidenced the outstanding catalytic performance of oxides containing manganese in different oxidation states ( $Mn_2O_3$ ,  $Mn_3O_4$  and  $MnO_x$ ) for the abatement of different VOCs like ethene, propene and toluene [20]. The latter study evidenced the beneficial role of surface-adsorbed electrophilic oxygen species and acidic sites in enhancing the catalytic activity.

In this work, a set of manganese oxide catalysts was synthesized via two different preparation techniques, the solution combustion (SCS) and the sol-gel (SG) syntheses. These procedures allowed the preparation of catalysts with different physicochemical and catalytic properties. The physico-chemical properties of the prepared powders catalysts were studied by means of several characterization techniques:  $N_2$ -physisorption at  $-196\text{ }^\circ\text{C}$ , X-ray powder diffraction,  $H_2$  temperature-programmed reduction, soot temperature-programmed reduction, X-ray photoelectron spectroscopy (XPS) and scanning electron microscopy (SEM). The high performance of the prepared catalysts was verified in the oxidation of VOC probe molecules (ethene and propene) and carbon soot.

## 2. MATERIALS AND METHODS

### 2.1 Catalysts preparation

The set of powder catalysts that were synthesized were composed by manganese oxide ( $MnO_x$ ). The catalysts were prepared by means of two preparation techniques: (i) the solution combustion synthesis (SCS) and (ii) the sol-gel (SG) synthesis. The different operative conditions applied in each procedure allowed the preparation of powder catalysts with different physico-chemical characteristics.

#### Solution combustion synthesis

During the preparation of the  $Mn_2O_3$  - SCS catalyst, an aqueous solution (50 mL) containing  $0.2\text{ mol L}^{-1}$  of the metal precursor, thus manganese nitrate tetrahydrate ( $Mn(NO_3)_2 \cdot 4H_2O$ , Sigma-Aldrich), and  $0.2\text{ mol L}^{-1}$  of citric acid (CA,  $C_6H_8O_7 \cdot H_2O$ , Sigma-Aldrich) was prepared. The solution was magnetically stirred for 10 min until the powders dissolved completely. Subsequently, the solution was heated in the oven from room temperature (r.t.) until  $650\text{ }^\circ\text{C}$  ( $5\text{ }^\circ\text{C min}^{-1}$ ), and calcined isothermally for 30 min. On the other hand, for the preparation of the  $Mn_3O_4/Mn_2O_3$  - SCS a molar ratio of 1:1.25 between the Mn nitrate and CA was assured in the solution. molar ratio. After the 10 min stirring,

the solution was heated from r.t. until 600 °C (10 °C min<sup>-1</sup>) and calcined at constant temperature for 30 min. Finally, the powders obtained were ground using mortar and pestle.

### Sol-gel synthesis

During the syntheses, manganese nitrate (0.2 mol L<sup>-1</sup>) was dissolved with CA (0.2 mol L<sup>-1</sup>) in 50 mL of Milli-Q water. After the powders were completely dissolved, the pH was increased (until pH = 5 was reached) by adding ammonium hydroxide (NH<sub>4</sub>OH, Sigma-Aldrich) dropwise. Afterwards, the solution was set in a water bath and the temperature was raised (ca. 1 °C min<sup>-1</sup>) until 60 °C under continuous stirring. The final temperature was maintained constant for 2 h to enhance the nucleation and aggregation of colloidal particles. Afterwards, the particles were separated from the suspension by means of vacuum filtration and were washed with water. The resulting solid was dried at 60 °C overnight. Subsequently, it was heated (5 °C min<sup>-1</sup>) in an oven from r.t. until: (i) 550 °C for the Mn<sub>2</sub>O<sub>3</sub> - SG550 and (ii) 650 °C for the Mn<sub>2</sub>O<sub>3</sub> - SG650. The resulting catalyst was gently ground using mortar and pestle.

### 2.2 Catalyst characterization

X-ray powder diffraction (XRD) analyses were performed by means of an X'Pert Philips PW3040 diffractometer. During the measurements, Cu K<sub>α</sub> radiation was utilized and the 2θ was varied in the 20° to 80° range; step = 0.05° 2θ and time per step = 0.2 s. The diffraction patterns harvested were indexed according to the Powder Data File (PDF 2000, International Centre of Diffraction Data, Pennsylvania) Database. The average size of the crystallites was estimated using the Scherrer formula,  $D = 0.9\lambda / b \cos \theta$ , where λ is the Cu K<sub>α</sub> radiation wavelength; 0.9 the shape factor for spherical particles; *b* the full width at half maximum (FWHM) in radians and θ the angle corresponding to the observed diffraction peak.

The specific surface area (S<sub>BET</sub>), the total pore volume and the pore diameter were calculated after the performance of N<sub>2</sub> physisorption at -196 °C technique (Micromeritics Tristar II 3020). Before carrying out the analysis, the powders were pretreated under a N<sub>2</sub> flow 200 °C for 2 h. The S<sub>BET</sub> were estimated by means of the Brunauer-Emmett-Teller (BET) method. The diameter and volume of the pores (D<sub>p</sub> and V<sub>p</sub>, respectively) were calculated using the method of Barrett-Joyner-Halenda (BJH) in the data corresponding to the desorption phase.

The morphology of the powder catalysts was observed by means of a field emission scanning electron microscope (FESEM) FEI QUANTA 200F, using the following operation parameters: HV = 10.00 kV, working distance = 4 - 5.4 mm, intensity = 46 - 180 nA.

The reducibility of the catalysts was investigated through the realization of H<sub>2</sub> temperature-programmed reduction (H<sub>2</sub>-TPR) in a ThermoQuest TPD/R/O 1100 analyzer. For the analyses, a thermal conductivity detector (TCD) was utilized. Prior to the performance of the analysis, the studied sample (ca. 20 mg) was subject to a pretreatment under a He flow (40 mL min<sup>-1</sup>) at 550 °C for 60 min. Subsequently, the temperature was lowered until r.t. and the analysis was started. During the analysis phase, the sample was reduced under a flow of 5 vol.%-H<sub>2</sub> in Ar (20 mL min<sup>-1</sup>) and the temperature was increased at a constant rate (5 °C min<sup>-1</sup>) from r.t. until 800 °C.

Soot-TPR technique was carried out to analyze the reducibility of the catalyst by soot. The technique was performed inside a quartz U-tube reactor (internal diameter ID = 4 mm), comprising a fixed-bed containing 45 mg of catalyst, 5 mg of soot and 150 mg of silica in “tight contact”. During the analysis, the temperature of the reactor was increased by means of a PID-controlled furnace. The intimate soot-catalyst contact condition (i.e. “tight contact”) was assured in a ball-milling apparatus operating at 250 rpm for 15 min. Before the reduction, the powder mix was pretreated under N<sub>2</sub> (100 mL min<sup>-1</sup>) at 100 °C for 30 min. After, the soot-TPR was carried out flowing N<sub>2</sub> (100 mL min<sup>-1</sup>) while the temperature was increased until 700 °C (5 °C min<sup>-1</sup>). The concentrations of CO<sub>2</sub> and CO in the reactor outlet were estimated by means of NDIR analyzers

X-ray photoelectron spectroscopy (XPS) investigations were conducted using an XPS PHI 5000 versa probe apparatus. The conditions applied during the analysis were a band-pass energy = 187.85 eV, size of the X-ray spot = 100 μm and take-off angle = 45°. The spectra obtained were fitted using the Multipack 9.0.

### 2.3 Catalytic activity tests

The catalytic activity of the powders was investigated a typical temperature-programmed oxidation setup. For the test, a fixed-bed containing the pelletized catalyst (diameter of pellets: 212-300  $\mu\text{m}$ ) was set in a quartz U-tube reactor (ID = 4 mm) and the temperature of the reactor was raised using a PID-controlled furnace. The temperature of the catalytic bed was estimated with a K-type thermocouple. The reactor outlet concentrations of CO and CO<sub>2</sub> were measured by non-dispersive infrared (NDIR) analyzers (ABB Uras 14).

### Total oxidation of VOC

Before the catalytic test, the catalyst (100 mg) was subjected to a degassing pretreatment under a flow of N<sub>2</sub> at 150 °C for 1 h. The gaseous mixture for the test was prepared by diluting the VOC (propene or ethene) in air in order to obtain a reactor inlet concentration of 500 ppm-VOC, 10 vol.%-O<sub>2</sub> and the balance in N<sub>2</sub>. The flow fed to the reactor was calculated according to a constant gas hourly space velocity (GHSV) of 20,000 h<sup>-1</sup>, equivalent to a weight-to-volumetric flowrate ratio (W/F) of 0.044 g h L<sup>-1</sup>. The isothermal steps (every 30 °C) performed during the analysis started at 70 °C, and the temperature was increased when a stable VOC conversion was observed (in terms of CO and CO<sub>2</sub> concentrations).

### Oxidation of soot

For the catalytic tests performed in “loose contact” between the catalyst and soot, 45 mg of catalyst, 5 mg of soot and 150 mg of inert silica were gently mixed with a spatula for 3 min. On the other hand, the “tight contact” catalyst-soot condition was obtained as described previously for the soot-TPR characterization procedure. The fixed-bed was pretreated under a flow of N<sub>2</sub> (100 mL min<sup>-1</sup>) at 100 °C for 30 min. Then, the catalytic test was carried out under gaseous flow (100 mL min<sup>-1</sup>) containing 10 vol.% of O<sub>2</sub> and the balance in N<sub>2</sub>. The temperature in the reactor was increased at a constant heating rate (5 °C min<sup>-1</sup>) from 100 °C until 700 °C.

## 3. RESULTS AND DISCUSSION

### 3.1 Material textural properties

In order to examine the crystalline phases present in the powder catalysts and their characteristics, XRD analyses were conducted. The diffraction patterns harvested during this technique are reported in **Figure 1**.

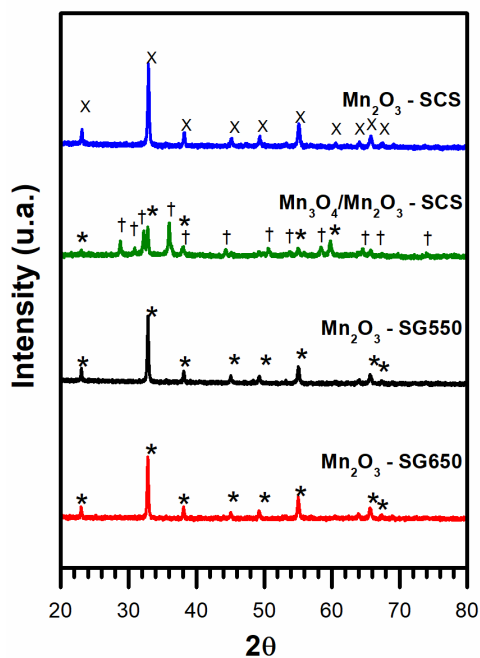


**Figure 1.** X-ray powder diffraction patterns of the synthesized catalysts. Assignments: Mn<sub>2</sub>O<sub>3</sub> peaks = X and \*; Mn<sub>3</sub>O<sub>4</sub> = †.

The patterns observed for the  $\text{Mn}_2\text{O}_3$ -SG550 and  $\text{Mn}_2\text{O}_3$ -SG650 consisted in the cubic structure of  $\text{Mn}_2\text{O}_3$  (reference code 01-078-0390). This demonstrates that, in spite of the different calcination temperatures used subsequently to the sol-gel preparation, the resulting crystalline phase consists in the system of  $\text{Mn}_2\text{O}_3$ . On the other hand, the pattern observed for the  $\text{Mn}_2\text{O}_3$  – SCS evidences the formation of the orthorhombic system of  $\text{Mn}_2\text{O}_3$  (ref. code 01-073-1826). Instead, the  $\text{Mn}_3\text{O}_4/\text{Mn}_2\text{O}_3$  catalyst showed a mixed diffraction pattern mainly composed by the pattern of hausmannite (ref. code 00-024-0734). However, additional diffraction lines appeared and were ascribed to the presence of  $\text{Mn}_2\text{O}_3$  (ref. code 01-078-0390).

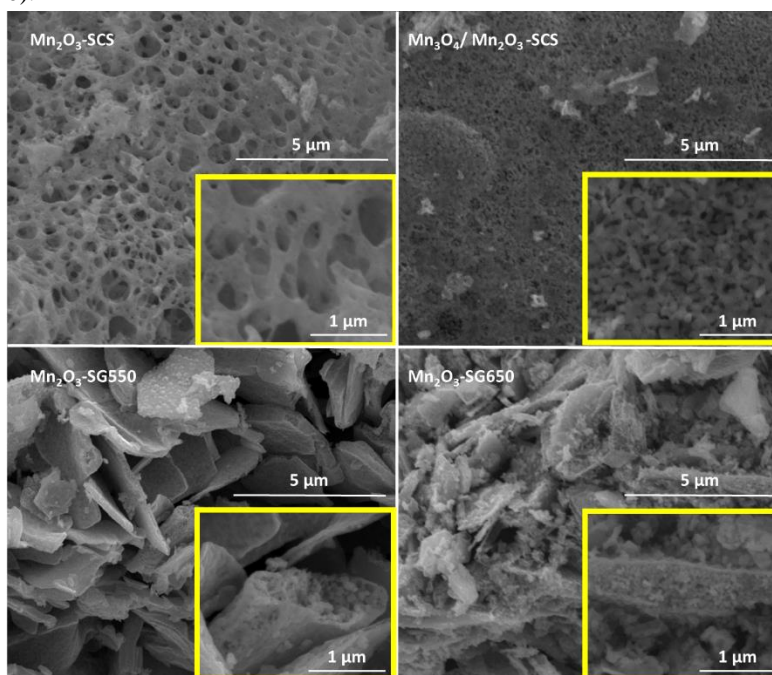


**Figure 2.** FESEM micrographs of the prepared catalysts and the corresponding magnifications (in the yellow frames).

The textural properties of the samples are summarized in **Table 1**. The results evidence that the SCS procedure allowed to obtain higher specific surface areas ( $S_{\text{BET}}$ ), with respect to the SG synthesis. Obviously, obtaining higher specific surface areas is a positive outcome since it may improve the catalytic performance in gas-phase reactions due to the higher amount of available active sites. On the other hand, a higher size of the crystallites was obtained in the samples prepared via the SG preparation respect to those obtained with the SCS technique.

**Table 1.** Textural properties of the synthesized catalysts calculated by means of the  $\text{N}_2$  physisorption at  $-196\text{ }^\circ\text{C}$  technique<sup>a</sup> and the Scherrer formula<sup>b</sup>.

Catalyst	$S_{\text{BET}}^{\text{a}}$ ( $\text{m}^2\text{ g}^{-1}$ )	$V_{\text{p}}^{\text{a}}$ ( $\text{cm}^3\text{ g}^{-1}$ )	$D_{\text{p}}^{\text{a}}$ (nm)	Crystallites size <sup>b</sup> (nm)
$\text{Mn}_2\text{O}_3$ -SG550	15	0.12	32	67
$\text{Mn}_2\text{O}_3$ -SG650	11	0.10	37	61
$\text{Mn}_2\text{O}_3$ -SCS	22	0.15	26	52
$\text{Mn}_3\text{O}_4/\text{Mn}_2\text{O}_3$ -SCS	21	0.13	23	37 / 53

The morphologies of the catalyst as observed in the FESEM are summarized in **Figure 2**. In general, the micrographs evidence the formation of mesoporous structures during both synthesis procedures. Moreover, the catalysts prepared

via SCS are characterized by a mesoporous structure. This coincides with the highest surface areas observed, thus suggesting the formation of highly porous “sponge-like” structures during the SCS technique. Instead, the morphology of the powders prepared via SG synthesis are formed by slim nanoplates. Interestingly, the micrographs evidence that the nanoplates formed in the sol-gel synthesis contain a porous interior enclosed in an external shell.

### 3.2 Temperature-programmed analyses

The reducibility of the catalysts was estimated under a flow of 5 vol.%-H<sub>2</sub> in Ar in the range 100-800 °C. The reduction profiles obtained are shown in **Figure 3**. As a general behaviour, the samples composed by Mn<sub>2</sub>O<sub>3</sub> evidenced a two-peak reduction profile. Therefore, in this case the reduction signal with maxima between 350-383 °C can be ascribed to the reduction step Mn<sub>2</sub>O<sub>3</sub> → Mn<sub>3</sub>O<sub>4</sub>, whereas the peak occurring at higher temperatures corresponds to the final reduction step Mn<sub>3</sub>O<sub>4</sub> → MnO [20,24–26]. Consistently, this result confirms the elevated amount of Mn species with oxidation state 3+ in the samples composed by Mn<sub>2</sub>O<sub>3</sub> (as observed during XRD analyses). Particularly, the formation of bigger particles in the SG synthesis (as estimated by means of Scherrer formula) seems related to a decreased intensity of the first reduction peak (i.e. the low-temperature peak), and the translation of the second signal to higher temperatures. According with the literature, this could be associated to the formation of bigger particles of Mn<sub>2</sub>O<sub>3</sub> which could be more resistant to reduction [27,28].

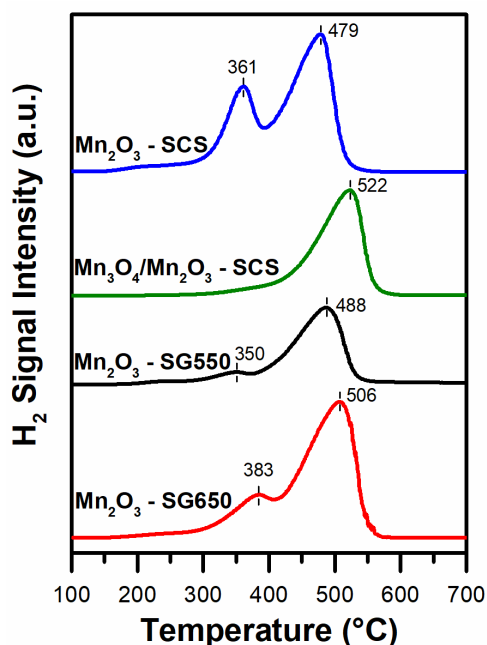


**Figure 3.** H<sub>2</sub>-TPR of the synthesized catalysts.

On the other hand, the small reduction signal of the Mn<sub>3</sub>O<sub>4</sub>/Mn<sub>2</sub>O<sub>3</sub> – SCS starting at ca. 300 °C may be attributed to the presence of Mn<sup>3+</sup> species in Mn<sub>2</sub>O<sub>3</sub> crystals, as confirmed in the XRD studies (vide supra). As a whole, a reducibility trend (in terms of low-temperature reduction signal) can be drawn as follows: Mn<sub>2</sub>O<sub>3</sub>-SG550 > Mn<sub>2</sub>O<sub>3</sub>-SCS > Mn<sub>2</sub>O<sub>3</sub>-SG650 > Mn<sub>3</sub>O<sub>4</sub>/Mn<sub>2</sub>O<sub>3</sub>-SCS.

The reducibility of the catalysts by soot in “tight contact” condition was studied in the absence of oxygen (see **Figure 4**). Under this condition, the oxidation of carbonaceous matter takes place by means of the oxygen species composing the catalyst. Various signal maxima of CO<sub>2</sub> appear in the whole range of temperature analyzed. The first signal (observed only for the Mn<sub>2</sub>O<sub>3</sub> – SG550) appeared at ca. 240 °C can be attributed to the desorption of CO<sub>2</sub> bonded to basic sites of manganese oxide [29]. On the other hand, the signal observed at T < 450 °C can be attributed to the oxidation of soot (C + O<sub>α</sub> → CO + O<sub>α</sub> → CO<sub>2</sub>) by means of chemisorbed O<sub>2</sub><sup>-</sup>, while the signal occurred between 450 and 550 °C is associated to other electrophilic oxygen species (e.g. O<sup>-</sup> and O<sub>2</sub><sup>2-</sup>) [30,31]. At higher temperatures the oxidation of soot occurs as a result of the release of oxygen present in the bulk (C + O<sub>β</sub> → CO + CO<sub>2</sub>), that coincides with the appearance of CO (see **Figure 4b**). The latter takes place due to the slow diffusion of oxygen from the bulk

to the surface, causing that some of the reaction intermediate (thus the CO) does not convert to CO<sub>2</sub> [32]. It is worth evidencing the lower signal intensity in the case of the catalysts calcined at 650 °C, respect to the signal of the Mn<sub>2</sub>O<sub>3</sub> – SG550. This result suggests that the higher calcination temperature may have stabilized the crystalline structure of the catalysts, thus leading to an overall lower reducibility. Consistently, the overall reducibility of the catalysts by soot follows the following trend: Mn<sub>2</sub>O<sub>3</sub>-SG550 > Mn<sub>2</sub>O<sub>3</sub>-SG650 ≈ Mn<sub>2</sub>O<sub>3</sub>-SCS ≈ Mn<sub>3</sub>O<sub>4</sub>/Mn<sub>2</sub>O<sub>3</sub>-SCS.

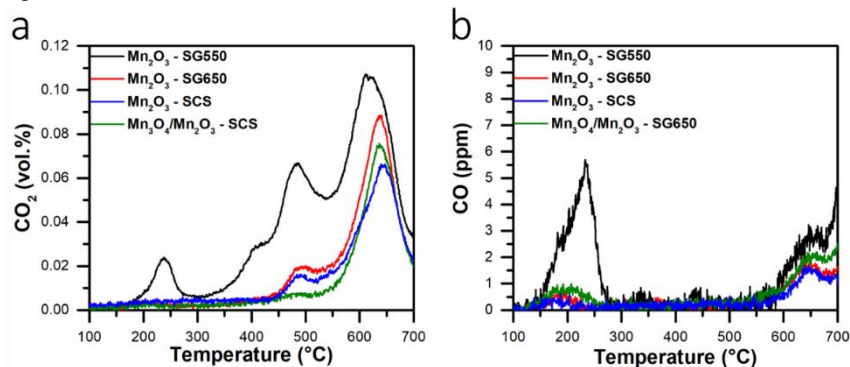


**Figure 4.** CO<sub>2</sub> (section a) and CO (section b) profiles observed during the soot-TPR analyses of the prepared catalysts.

### 3.3 X-ray photoelectron spectroscopy

The spectra obtained during the XPS investigations are summarized in Figure 5. The spectra obtained in the O 1s core level and the respective deconvolution are shown in Figure 5a. As a whole, the spectra are characterized by a signal with two maxima at different binding energy (BE) values, each one assigned to different oxygen species. The signal appeared at low binding energy (between 529.6 and 529.9 eV) are attributed to nucleophilic lattice oxygen (O<sup>2-</sup>) bonded to Mn (thus O<sub>β</sub> species) [33]. On the other hand, the signal maxima centered between 531.2 and 531.4 eV is ascribed to electrophilic oxygen species (e.g. O<sup>-</sup> or O<sub>2</sub><sup>-</sup>) or OH groups located over the surface of the catalyst [21,34]. The amount of O<sub>α</sub> and O<sub>β</sub> species (see Table 2) were estimated according to the deconvolution of the spectra. A decreasing trend of the O<sub>α</sub>/O<sub>β</sub> ratio was observed as follows: Mn<sub>2</sub>O<sub>3</sub>-SG550 > Mn<sub>2</sub>O<sub>3</sub>-SCS > Mn<sub>2</sub>O<sub>3</sub>-SG650 ≈ Mn<sub>3</sub>O<sub>4</sub>/Mn<sub>2</sub>O<sub>3</sub>-SCS. Remarkably, the increased amount of O<sub>α</sub> has been correlated in the literature to total oxidation of hydrocarbons [20,35,36].

**Table 2.** Relative percentages (at.%) of oxygen species calculated from the deconvolution of the O 1s XPS spectra.

Catalyst	O <sub>α</sub> , OH <sup>-</sup> BE (eV)	O <sub>α</sub> (at.%)	O <sub>β</sub> BE (eV)	O <sub>β</sub> (at.%)	O <sub>α</sub> /O <sub>β</sub>
Mn <sub>2</sub> O <sub>3</sub> -SG550	531.4	56.7	529.8	43.3	1.31
Mn <sub>2</sub> O <sub>3</sub> -SG650	531.2	31.8	529.6	68.2	0.47
Mn <sub>2</sub> O <sub>3</sub> -SCS	531.3	38.5	529.6	61.5	0.63
Mn <sub>3</sub> O <sub>4</sub> /Mn <sub>2</sub> O <sub>3</sub> -SCS	531.4	31.8	529.9	68.2	0.47

Additionally, the XP spectra in the Mn 2p core level were measured and are included in Figure 5b. The signal observed at higher binding energy is attributed to the 2p<sub>1/2</sub> level, whereas the signal located at lower binding energy (between 637.8–647.4 eV) corresponds to the 2p<sub>3/2</sub> level. As reported in the literature, the deconvolution of the latter signal can be used for estimating the relative amount of Mn<sup>x+</sup> species (where x = 2+, 3+ and 4+) in the sample [20,21,37]. The spectra deconvolution (numerical data not reported for the sake of brevity) confirmed the predominance of Mn species with oxidation state 3+ for the samples composed mainly by Mn<sub>2</sub>O<sub>3</sub>. Instead, the calculations on the amount of Mn<sup>3+</sup> and Mn<sup>2+</sup> evidenced, as expected, rather similar abundances for the sample composed by the spinel Mn<sub>3</sub>O<sub>4</sub>.

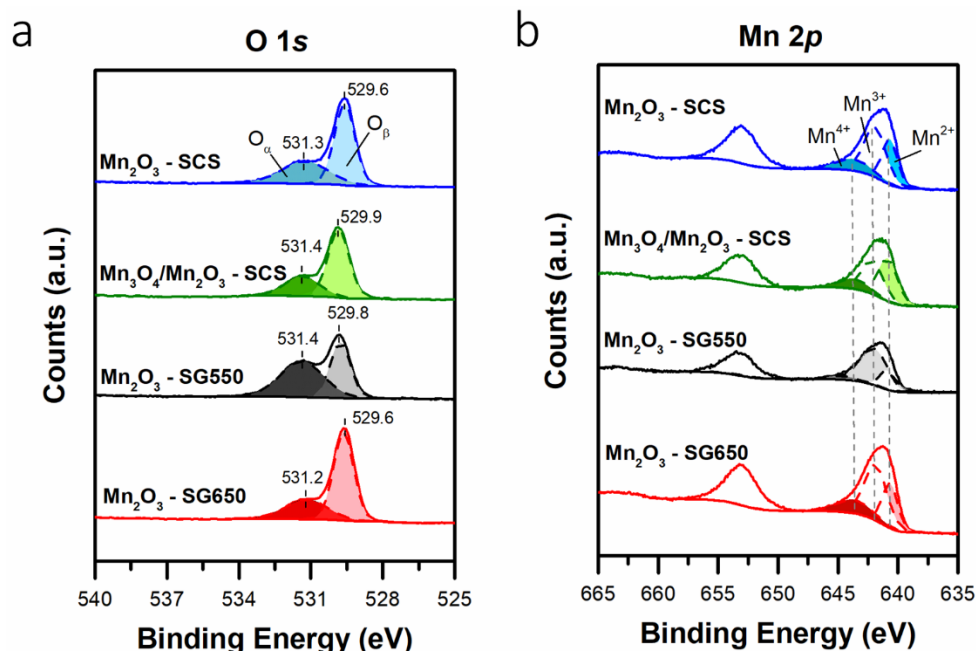


**Figure 5.** XPS spectra in the O 1s (section a) and Mn 2p core level (section b).

### 3.4 Catalytic activity: Oxidation of VOCs

The catalytic performance of the prepared catalysts was evaluated in the oxidation of carbon soot precursors (i.e. volatile organic compounds). During the testing of the samples, propene and ethene were used as probe VOC molecules. The catalytic performances observed during the tests are summarized in Figure 6,7 (section a). The whole set of catalysts converted completely the VOCs at lower temperatures respect to the blank test with no catalyst. The VOC conversion rates of the prepared catalysts are summarized in Table 3.

**Table 3.** Propene and ethene specific reaction rates over the prepared catalysts.

Catalyst	$r_{\text{propene}}^a$ ( $\mu\text{mol h}^{-1} \text{m}^{-2}$ )	$r_{\text{ethene}}^b$ ( $\mu\text{mol h}^{-1} \text{m}^{-2}$ )
Mn <sub>2</sub> O <sub>3</sub> -SG550	0.94	1.67
Mn <sub>2</sub> O <sub>3</sub> -SG650	0.49	1.13
Mn <sub>2</sub> O <sub>3</sub> -SCS	0.35	1.04
Mn <sub>3</sub> O <sub>4</sub> /Mn <sub>2</sub> O <sub>3</sub> -SCS	1.48	1.69

<sup>a</sup> calculated at 130 °C, <sup>b</sup> calculated at 160 °C

The following trend can be outlined for the catalytic activity during the oxidation of propene: Mn<sub>3</sub>O<sub>4</sub>/Mn<sub>2</sub>O<sub>3</sub>-SCS > Mn<sub>2</sub>O<sub>3</sub>-SG550 > Mn<sub>2</sub>O<sub>3</sub>-SCS > Mn<sub>2</sub>O<sub>3</sub>-SG650. The general performances of the catalysts prepared via SG evidence a catalytic improvement when a lower calcination temperature is utilized. In fact, the higher temperature may have caused the sintering of the catalyst, leading to the reduction of the catalyst's surface area (as reported in Table 1). Therefore, this finding confirms the key role of the calcination temperature for the preparation of catalysts active in the oxidation of VOCs. The most active catalyst in the oxidation of propene is composed mainly by the spinel structure Mn<sub>3</sub>O<sub>4</sub> (coupled Mn<sup>3+</sup>/Mn<sup>2+</sup> species) with the smallest crystallite size of the prepared set of catalysts (ca. 37 nm for the Mn<sub>3</sub>O<sub>4</sub>). In this sense, the outstanding activity of the Mn<sub>3</sub>O<sub>4</sub>/Mn<sub>2</sub>O<sub>3</sub>-SCS catalyst could be associated with the

presence of small crystallites of hausmannite that, according to the literature, can promote an elevated occurrence of crystallite edge and corners, and thus more defective structures active in the oxidation reaction [38,39]. It is worth noting that among the catalysts classified as pure  $Mn_2O_3$  (by means of XRD), the catalytic trend coincides with a decreasing behaviour of two parameters: (i) the low-temperature reducibility, and (ii) with the amount of surface chemisorbed  $O_\alpha$ -species. In fact, the catalytic performance data were fitted and evidenced a linear behaviour dependent on the low-temperature reduction peak (see Figure 6b), thus confirming the correlation between the reducibility and the improved catalytic activity in propene oxidation (in terms of  $T_{10\%}$ ,  $T_{50\%}$  and  $T_{90\%}$ , thus the temperatures for achieving a conversion of 10%, 50% and 90%, respectively).

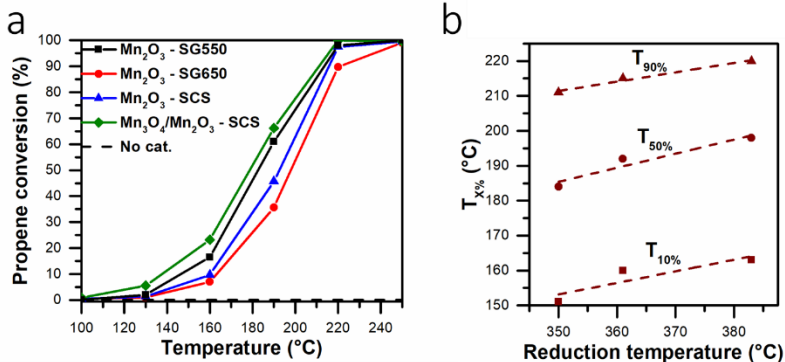


**Figure 6.** Catalytic performances in the oxidation of  $C_3H_6$  (section a) and correlation between the low-temperature reduction peak and the catalytic performance in  $C_3H_6$  oxidation (over  $Mn_2O_3$  catalysts) in terms of  $T_{10\%}$ ,  $T_{50\%}$  and  $T_{90\%}$  (section b).

On the other hand, the  $Mn_2O_3$ -SG550 catalyst is spite of having an intermediate value of surface area (respect to the whole set of catalysts), showed the best overall catalytic performance in the abatement of ethene (see Figure 7a). Considering the overall catalytic performance and the low-temperature ethene reaction rates, the following catalytic activity trend in the oxidation of ethene can be drawn:  $Mn_2O_3$ -SG550 >  $Mn_2O_4/Mn_2O_3$ -SCS >  $Mn_2O_3$ -SCS >  $Mn_2O_3$ -SG650. As a whole, the catalytic activity seems attributable to: the relative amount of active chemisorbed  $O_\alpha$ -species (as verified via XPS, vide supra) and (in case of the  $Mn_2O_3$  catalysts) the low-temperature reducibility of the catalysts (see Figure 7b).

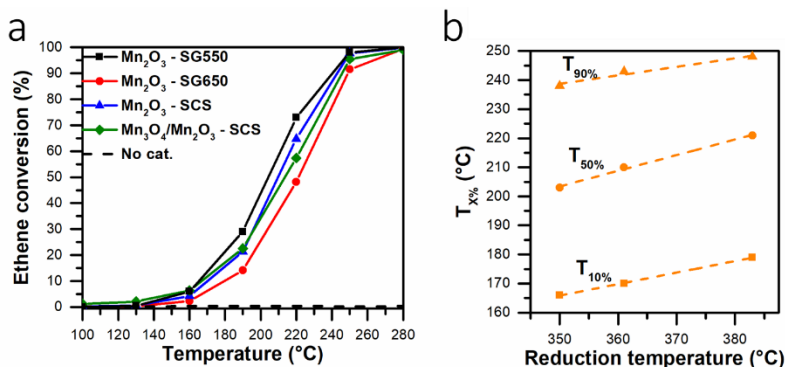


**Figure 7.** Catalytic performances in the oxidation of  $C_2H_4$  (section a) and correlation between the low-temperature reduction peak and the catalytic performance in  $C_2H_4$  oxidation (over  $Mn_2O_3$  catalysts) in terms of  $T_{10\%}$ ,  $T_{50\%}$  and  $T_{90\%}$  (section b).

Accordingly, the results evidence the key role played by active  $O_\alpha$ -species and the catalyst reducibility in the elimination of ethene. In fact, a high amount of these species and the low-temperature reducibility, according to the literature, may promote VOC catalytic oxidation at lower temperatures [20,21,27,40]. Overlooking the catalytic behaviour observed during the abatement of the VOCs, it is evident how catalysts that belong to the same group or family may present different catalytic performances according to the abated molecule. In other words, it is evidenced how the catalytic activity for a specific reaction may depend on a wide set of physico-chemical properties (reducibility, surface acidity, size of crystallites, amount of chemisorbed oxygen species, etc.). Consequently, it may be speculative

to select a catalyst for a specific reaction, according to a single physico-chemical property or to catalytic results obtained with other molecules. In conclusion, the prepared catalysts showed a high catalytic activity at relatively low temperatures in the elimination of VOCs, i.e. carbon soot precursors, at relatively low temperatures.

### 3.5 Catalytic activity: Oxidation of carbonaceous matter (soot)

The catalytic activity of the oxides was tested in the oxidation of carbonaceous matter in “loose” or “tight” contact. The former condition was assured by a delicate mixing of the powders (soot, catalyst, inert silica), whereas the most intimate solid-solid interaction (i.e. “tight” contact) were enhanced by means of the ball milling process. The curves of the soot catalytic conversions of the prepared catalysts are included in Figure 8.

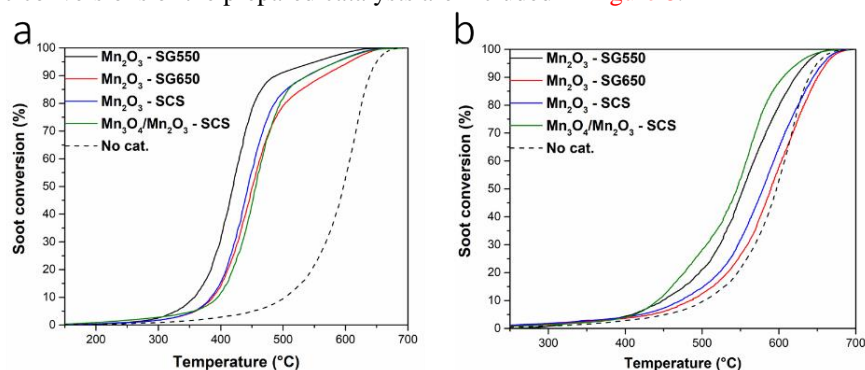


**Figure 8.** Catalytic conversion of carbon soot as a function of the temperature in (a) “loose” and (b) “tight” contact conditions

During all the catalytic tests, CO<sub>2</sub> was the main oxidation product, while the concentration of CO remained low (or even imperceptible) in most cases. The soot oxidation is a solid-solid reaction, therefore, enhancing the catalyst-soot contact plays a key role for estimating soot oxidation kinetics [41]. In this sense, the conversions obtained in “tight” condition evidence the intrinsic activity of the catalytic surface. Consistently, the results obtained in “tight” contact evidence that the catalytic performance of the active phase in the catalysts calcined at higher temperatures ( $T > 600$  °C, see the blue, red and green lines) are rather similar. Instead, the best performance was observed in the catalyst calcined at the lowest temperature, *ca.* 550 °C (*i.e.* the Mn<sub>2</sub>O<sub>3</sub> – SG550). This catalyst achieved 10% and 50% of the soot conversion at temperatures approx. 25 °C below the other catalysts. These results suggest that the higher calcination temperatures may have enhanced a sintering process that diminished the whole number of soot-MnO<sub>x</sub> contact points present in the catalysts. On the other hand, the reducibility of the catalysts was diminished in the catalysts calcined at higher temperatures (as demonstrated by soot-TPR analyses, *vide supra*), which can be as well correlated with their lower catalytic performance in “tight” contact conditions. Furthermore, the best catalyst contained the highest amount of active O<sub>α</sub>-species, important for starting soot oxidation [18]. Therefore, demonstrating the remarkable importance of an elevated amount of surface O<sub>α</sub> species and an improved reducibility of the catalyst in the carbon soot oxidation process.

The “loose” contact conditions are more representative of real contact conditions in catalytic traps [41]. The results evidence similar catalytic activities for the Mn<sub>2</sub>O<sub>3</sub> – SG650 and the Mn<sub>2</sub>O<sub>3</sub> – SCS. However, under this contact condition the soot conversion of the catalyst containing the spinel Mn<sub>3</sub>O<sub>4</sub> overcomes the catalytic performance of the Mn<sub>2</sub>O<sub>3</sub> – SG550. This suggests that in spite of the higher temperature treatment of the former catalyst, the contact points between soot and Mn<sub>3</sub>O<sub>4</sub> greatly enhance the catalytic performance. Accordingly, this evidences that the contact points are readily accessible for the soot without favouring an intimate soot-catalyst contact. This can be associated to the sponge-like morphology of the catalyst, characteristic of the SCS preparation technique. This morphology resembles a catalytic trap or a filter. In this case, it may allow an easier path for soot to penetrate the structure of the catalyst and remain trapped inside it, respect to the void nanoplates. Accordingly, this may enhance the occurrence of contact points for the catalytic oxidation of soot. Moreover, in previous studies, Mn<sub>3</sub>O<sub>4</sub> (and mixed oxides containing Mn<sub>3</sub>O<sub>4</sub>) demonstrated to host an increased amount of acid sites respect to other MnO<sub>x</sub> [20,42]. The Lewis acid sites are characterized by superficial (oxygen deficient) metal cations. These sites can play a key role in the adsorption of the oxygen needed for the oxidation reaction, its surface diffusion and the final transfer to soot and, therefore, are can

be correlated to the soot oxidation performance [43,44]. Consistently, the elevated activity in “loose” catalyst-soot contact was ascribed to the combined promoting effects of the sponge-type morphology (acting like a powder filter or trap) and a probable increased amount of acid sites that are in contact with soot of the  $Mn_3O_4/Mn_2O_3$ -SCS catalyst. The overall results demonstrate the remarkable effectivity of sustainable  $MnO_x$  based oxides in the elimination of not only solid carbon soot, but also its organic precursors, *i.e.* the VOCs.

#### 4. CONCLUSIONS

A set of manganese oxide catalysts was synthesized via two preparation techniques, the solution combustion synthesis ( $Mn_3O_4/Mn_2O_3$ -SCS and  $Mn_2O_3$ -SCS) and the sol-gel synthesis ( $Mn_2O_3$  – SG550 and  $Mn_2O_3$  – SG650). These synthesis procedures allowed the preparation of catalysts with different physico-chemical and catalytic properties. Overall, the best catalytic performances in the abatement of solid carbon soot and VOCs, were observed in the  $Mn_2O_3$  – SG550 and the  $Mn_3O_4/Mn_2O_3$ -SCS catalysts. Concerning the catalytic oxidation of the studied VOCs, the best catalytic performances were associated to the following parameters:

- (i) The elevated relative amounts of active surface  $O_\alpha$  species, that can improve significantly the activity in catalytic total oxidation of hydrocarbons at low temperatures.
- (ii) The improved low-temperature reducibility of the catalysts, due to the enhanced mobility of oxygen that takes part in the oxidation reactions.
- (iii) The appearance of small crystallites, which may contain an elevated amount of surface defects that enhance the catalytic performance.

The mentioned characteristics (i and ii) evidenced their influence on the oxidative performance of the catalysts in the solid carbon soot oxidation reaction. Accordingly, in “tight” contact condition, the best catalytic performance in soot oxidation was observed in the catalyst containing the highest amount of  $O_\alpha$  species and the better reducibility of the catalyst, *i.e.* the  $Mn_2O_3$  – SG550. This result highlights the beneficial effect of those two parameters in the intrinsic oxidative activity of the catalysts surface. Whereas the outstanding catalytic activity of the  $Mn_3O_4/Mn_2O_3$ -SCS in “loose” contact was attributed to the combined effect of: (i) a filter-like morphology (that may improve the capture of soot particles) and (ii) a probable high amount of surface acid sites that are characteristic of  $Mn_3O_4$  catalysts.

#### 5. REFERENCES

- [1] P. Sicard, Y.O. Khaniabadi, S. Perez, M. Gualtieri, A. De Marco, Effect of O<sub>3</sub>, PM<sub>10</sub> and PM<sub>2.5</sub> on cardiovascular and respiratory diseases in cities of France, Iran and Italy, *Environ. Sci. Pollut. Res.* 26 (2019) 32645–32665. <https://doi.org/10.1007/s11356-019-06445-8>.
- [2] J. Spiteri, P. von Brockdorff, Transboundary air pollution and respiratory disease mortality: evidence from European countries, *J. Econ. Stud.* (2020). <https://doi.org/10.1108/JES-05-2020-0210>.
- [3] G. Viegi, S. Baldacci, S. Maio, S. Fasola, I. Annesi-Maesano, F. Pistelli, L. Carrozzi, S. La Grutta, F. Forastiere, Health effects of air pollution: a Southern European perspective, *Chin. Med. J. (Engl)*. 133 (2020) 1568–1574. <https://doi.org/10.1097/CM9.0000000000000869>.
- [4] K. Vohra, A. Vodonos, J. Schwartz, E.A. Marais, M.P. Sulprizio, L.J. Mickley, Global mortality from outdoor fine particle pollution generated by fossil fuel combustion: Results from GEOS-Chem, *Environ. Res.* 195 (2021) 110754. <https://doi.org/10.1016/j.envres.2021.110754>.
- [5] European Parliament and Council, DIRECTIVE 2008/50/EC OF THE EUROPEAN PARLIAMENT AND OF THE COUNCIL of 21 May 2008 on ambient air quality and cleaner air for Europe, 2008. <https://eur-lex.europa.eu/legal-content/EN/TXT/?qid=1600695099487&uri=CELEX:02008L0050-20150918> (accessed January 21, 2021).
- [6] United States Environmental Protection Agency, Particulate Matter (PM) Implementation Regulatory Actions | Particulate Matter (PM) Pollution | US EPA, (2019). <https://www.epa.gov/pm-pollution/particulate-matter-pm-implementation-regulatory-actions> (accessed September 21, 2020).
- [7] R. Koppmann, Volatile organic compounds in the atmosphere, Blackwell Pub, 2007.
- [8] S. Mohankumar, P. Senthilkumar, Particulate matter formation and its control methodologies for diesel engine: A comprehensive review, *Renew. Sustain. Energy Rev.* 80 (2017) 1227–1238. <https://doi.org/10.1016/j.rser.2017.05.133>.
- [9] T. Gupta, D. Kumar Singh, Organic Species Emitted as a Part of Combustion Residue: Fate and Transformation in the Ambient Air Critical microenvironment View project Design innovation View project Organic Species Emitted as a Part of Combustion Residue: Fate and Transformation in the Ambient Air, 2016. <https://www.researchgate.net/publication/298392042> (accessed September 21, 2020).
- [10] T. Gelles, A. Krishnamurthy, B. Adebayo, A. Rownaghi, F. Rezaei, Abatement of gaseous volatile organic compounds: A material perspective, *Catal. Today.* 350 (2020) 3–18. <https://doi.org/10.1016/j.cattod.2019.06.017>.
- [11] X. Li, L. Zhang, Z. Yang, P. Wang, Y. Yan, J. Ran, Adsorption materials for volatile organic compounds (VOCs) and the key factors for VOCs adsorption process: A review, *Sep. Purif. Technol.* 235 (2020) 116213. <https://doi.org/10.1016/j.seppur.2019.116213>.
- [12] C. Yang, G. Miao, Y. Pi, Q. Xia, J. Wu, Z. Li, J. Xiao, Abatement of various types of VOCs by adsorption/catalytic oxidation: A review, *Chem. Eng. J.* 370 (2019) 1128–1153. <https://doi.org/10.1016/j.cej.2019.03.232>.
- [13] M.S. Kamal, S.A. Razzak, M.M. Hossain, Catalytic oxidation of volatile organic compounds (VOCs) – A review, *Atmos. Environ.* 140 (2016) 117–134. <https://doi.org/10.1016/j.atmosenv.2016.05.031>.

- [14] M. Schiavon, V. Torretta, A. Casazza, M. Ragazzi, Non-thermal Plasma as an Innovative Option for the Abatement of Volatile Organic Compounds: a Review, *Water, Air, Soil Pollut.* 228 (2017) 1–20. <https://doi.org/10.1007/s11270-017-3574-3>.
- [15] S. K. P. Veerapandian, N. De Geyter, J.-M. Giraudon, J.-F. Lamonier, R. Morent, The Use of Zeolites for VOCs Abatement by Combining Non-Thermal Plasma, Adsorption, and/or Catalysis: A Review, *Catalysts*. 9 (2019) 98. <https://doi.org/10.3390/catal9010098>.
- [16] A. Krishnamurthy, B. Adebayo, T. Gelles, A. Rownaghi, F. Rezaei, Abatement of gaseous volatile organic compounds: A process perspective, *Catal. Today*. 350 (2020) 100–119. <https://doi.org/10.1016/j.cattod.2019.05.069>.
- [17] F.I. Khan, A. Kr. Ghoshal, Removal of Volatile Organic Compounds from polluted air, *J. Loss Prev. Process Ind.* 13 (2000) 527–545. [https://doi.org/10.1016/S0950-4230\(00\)00007-3](https://doi.org/10.1016/S0950-4230(00)00007-3).
- [18] D. Fino, S. Bensaid, M. Piumetti, N. Russo, A review on the catalytic combustion of soot in Diesel particulate filters for automotive applications: From powder catalysts to structured reactors, *Appl. Catal. A Gen.* 509 (2016) 75–96. <https://doi.org/10.1016/j.apcata.2015.10.016>.
- [19] Z. Zhang, Z. Jiang, W. Shanguan, Low-temperature catalysis for VOCs removal in technology and application: A state-of-the-art review, *Catal. Today*. 264 (2016) 270–278. <https://doi.org/10.1016/j.cattod.2015.10.040>.
- [20] M. Piumetti, D. Fino, N. Russo, Mesoporous manganese oxides prepared by solution combustion synthesis as catalysts for the total oxidation of VOCs, *Appl. Catal. B Environ.* 163 (2015) 277–287. <https://doi.org/10.1016/j.apcatb.2014.08.012>.
- [21] V.P. Santos, M.F.R. Pereira, J.J.M. Órfão, J.L. Figueiredo, The role of lattice oxygen on the activity of manganese oxides towards the oxidation of volatile organic compounds, *Appl. Catal. B Environ.* 99 (2010) 353–363. <https://doi.org/10.1016/j.apcatb.2010.07.007>.
- [22] J.J. Spivey, Complete catalytic oxidation of volatile organics, *Ind. Eng. Chem. Res.* 26 (1987) 2165–2180. <https://doi.org/10.1021/ie00071a001>.
- [23] W.M. Haynes, *CRC Handbook of Chemistry and Physics : A Ready-Reference Book of Chemical and Physical Data.*, 95th ed., 2014.
- [24] D.A. Aguilera, A. Perez, R. Molina, S. Moreno, Cu-Mn and Co-Mn catalysts synthesized from hydrotalcites and their use in the oxidation of VOCs, *Appl. Catal. B Environ.* 104 (2011) 144–150. <https://doi.org/10.1016/j.apcatb.2011.02.019>.
- [25] D. Delimaris, T. Ioannides, VOC oxidation over MnOx-CeO2 catalysts prepared by a combustion method, *Appl. Catal. B Environ.* 84 (2008) 303–312. <https://doi.org/10.1016/j.apcatb.2009.02.003>.
- [26] F. Kaptejin, L. Singoredjo, A. Andreini, J.A. Moulijn, Activity and selectivity of pure manganese oxides in the selective catalytic reduction of nitric oxide with ammonia, *Appl. Catal. B Environ.* 3 (1994) 173–189. [https://doi.org/10.1016/0926-3373\(93\)E0034-9](https://doi.org/10.1016/0926-3373(93)E0034-9).
- [27] M. Piumetti, S. Bensaid, T. Andana, N. Russo, R. Pirone, D. Fino, Cerium-copper oxides prepared by solution combustion synthesis for total oxidation reactions: From powder catalysts to structured reactors, *Appl. Catal. B Environ.* 205 (2017) 455–468. <https://doi.org/10.1016/j.apcatb.2016.12.054>.
- [28] D. Delimaris, T. Ioannides, VOC oxidation over CuO-CeO2 catalysts prepared by a combustion method, *Appl. Catal. B Environ.* 89 (2009) 295–302. <https://doi.org/10.1016/j.apcatb.2009.02.003>.
- [29] A.R. Gandhe, J.S. Rebello, J.L. Figueiredo, J.B. Fernandes, Manganese oxide OMS-2 as an effective catalyst for total oxidation of ethyl acetate, *Appl. Catal. B Environ.* 72 (2007) 129–135. <https://doi.org/10.1016/j.apcatb.2006.10.017>.
- [30] R. Spinicci, A. Tofanari, Characterization of catalysts for methane-coupling by means of temperature programmed desorption, *Catal. Today*. 6 (1990) 473–479. [https://doi.org/10.1016/0920-5861\(90\)85041-L](https://doi.org/10.1016/0920-5861(90)85041-L).
- [31] Z. Li, M. Meng, Y. Zha, F. Dai, T. Hu, Y. Xie, J. Zhang, Highly efficient multifunctional dually-substituted perovskite catalysts La<sub>1-x</sub>KxCo<sub>1-y</sub>Cu<sub>y</sub>O<sub>3-δ</sub> used for soot combustion, NOx storage and simultaneous NOx-soot removal, *Appl. Catal. B Environ.* 121–122 (2012) 65–74. <https://doi.org/10.1016/j.apcatb.2012.03.022>.
- [32] T. Andana, M. Piumetti, S. Bensaid, N. Russo, D. Fino, R. Pirone, Nanostructured ceria-praseodymia catalysts for diesel soot combustion, *Appl. Catal. B Environ.* 197 (2016) 125–137. <https://doi.org/10.1016/j.apcatb.2015.12.030>.
- [33] J.F. Moulder, W.F. Stickle, P.E. Sobol, K.D. Bomben, *Handbook of X-ray Photoelectron Spectroscopy*, Perkin-Elmer Corporation, Physical Electronics Division, Eden Prairie, United States of America, 1992.
- [34] S.C. Kim, W.G. Shim, Catalytic combustion of VOCs over a series of manganese oxide catalysts, *Appl. Catal. B Environ.* 98 (2010) 180–185. <https://doi.org/10.1016/j.apcatb.2010.05.027>.
- [35] Y. Liu, H. Dai, J. Deng, S. Xie, H. Yang, W. Tan, W. Han, Y. Jiang, G. Guo, Mesoporous Co<sub>3</sub>O<sub>4</sub>-supported gold nanocatalysts: Highly active for the oxidation of carbon monoxide, benzene, toluene, and o-xylene, *J. Catal.* 309 (2014) 408–418. <https://doi.org/10.1016/j.jcat.2013.10.019>.
- [36] M. Zawadzki, J. Trawczyński, Synthesis, characterization and catalytic performance of LSCF perovskite for VOC combustion, in: *Catal. Today*, Elsevier, 2011; pp. 449–452. <https://doi.org/10.1016/j.cattod.2010.10.070>.
- [37] M.C. Biesinger, B.P. Payne, A.P. Grosvenor, L.W.M. Lau, A.R. Gerson, R.S.C. Smart, Resolving surface chemical states in XPS analysis of first row transition metals, oxides and hydroxides: Cr, Mn, Fe, Co and Ni, *Appl. Surf. Sci.* 257 (2011) 2717–2730. <https://doi.org/10.1016/j.apsusc.2010.10.051>.
- [38] M. Piumetti, N. Russo, Notes on Catalysis for Environment and Energy, CLUT-Politecnico di Torino, 2017.
- [39] M. Dosa, M. Piumetti, S. Bensaid, T. Andana, C. Novara, F. Giorgis, D. Fino, N. Russo, Novel Mn–Cu-Containing CeO<sub>2</sub> Nanopolyhedra for the Oxidation of CO and Diesel Soot: Effect of Dopants on the Nanostructure and Catalytic Activity, *Catal. Letters*. 148 (2018) 298–311. <https://doi.org/10.1007/s10562-017-2226-y>.
- [40] M.J. Marin Figueiredo, T. Andana, S. Bensaid, M. Dosa, D. Fino, N. Russo, M. Piumetti, Cerium–Copper–Manganese Oxides Synthesized via Solution Combustion Synthesis (SCS) for Total Oxidation of VOCs, *Catal. Letters*. 150 (2020) 1821–1840. <https://doi.org/10.1007/s10562-019-03094-x>.
- [41] M. Piumetti, B. van der Linden, M. Makkee, P. Miceli, D. Fino, N. Russo, S. Bensaid, Contact dynamics for a solid-solid reaction mediated by gas-phase oxygen: Study on the soot oxidation over ceria-based catalysts, *Appl. Catal. B Environ.* 199 (2016) 96–107. <https://doi.org/10.1016/j.apcatb.2016.06.006>.
- [42] F.A. Deorsola, S. Andreoli, M. Armandi, B. Bonelli, R. Pirone, Unsupported nanostructured Mn oxides obtained by Solution Combustion Synthesis: Textural and surface properties, and catalytic performance in NOx SCR at low temperature, *Appl. Catal. A Gen.* 522 (2016) 120–129. <https://doi.org/10.1016/j.apcata.2016.05.002>.
- [43] S. Wagloehner, M. Nitzler-Noski, S. Kureti, Oxidation of soot on manganese oxide catalysts, *Chem. Eng. J.* 259 (2015) 492–504. <https://doi.org/10.1016/j.cej.2014.08.021>.
- [44] S. Wagloehner, J.N. Baer, S. Kureti, Structure-activity relation of iron oxide catalysts in soot oxidation, *Appl. Catal. B Environ.* 147 (2014) 1000–1008. <https://doi.org/10.1016/j.apcatb.2013.09.049>.